Journal Pre-proofs

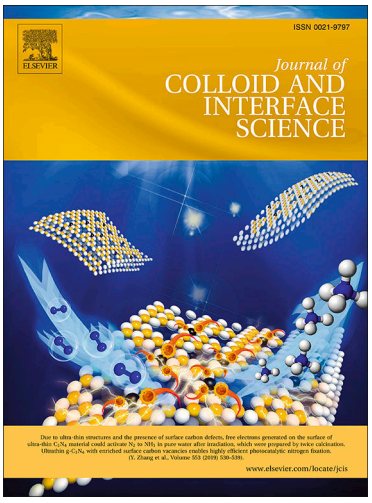

Role of ion exchange membranes and capacitive electrodes in Membrane Capacitive Deionization (MCDI) for CO_2 capture

L. Legrand, Q. Shu, M. Tedesco, J.E. Dykstra, H.V.M. Hamelers

PII: S0021-9797(19)31498-5
DOI: https://doi.org/10.1016/j.jcis.2019.12.039
Reference: YJCIS 25779

To appear in: *Journal of Colloid and Interface Science*

Received Date: 19 September 2019
Revised Date: 10 December 2019
Accepted Date: 11 December 2019

Please cite this article as: L. Legrand, Q. Shu, M. Tedesco, J.E. Dykstra, H.V.M. Hamelers, Role of ion exchange membranes and capacitive electrodes in Membrane Capacitive Deionization (MCDI) for CO_2 capture, *Journal of Colloid and Interface Science* (2019), doi: https://doi.org/10.1016/j.jcis.2019.12.039

Role of ion exchange membranes and capacitive electrodes in Membrane Capacitive Deionization (MCDI) for CO_2 capture

L. Legrand[a,b], Q. Shu[a,b], M. Tedesco[a], J.E. Dykstra[b], H.V.M. Hamelers[a]

[a] Wetsus, European Centre of Excellence for Sustainable Water Technology, Oostergoweg 9, 8911 MA Leeuwarden, the Netherlands

[b] Environmental Technology, Wageningen University, Bornse Weilanden 9, 6708 WG Wageningen, the Netherlands

Corresponding author (H.V.M. Hamelers): bert.hamelers@wetsus.nl, +31(0)58 284 30 00

Abstract

Recently we showed that membrane capacitive deionization (MCDI) can be used to capture CO_2, but we found that the performance decreases with decreasing current density. In the present study, we investigate the effect of electrodes and ion exchange membranes by performing experiments with two membranes (CO_2-MCDI), with one membrane (cation or anion exchange membrane), and without membranes (CO_2-CDI). We find that the anion exchange membrane is essential to keep high CO_2 absorption efficiencies ($\Lambda_a = n_{CO_2(g)}/n_{charge}$), while the absorption efficiency of the CO_2-CDI cell was lower than expected ($\Lambda_a \approx 0.5$ for CO_2-MCDI against $\Lambda_a \approx 0.18$ for CO_2-CDI). Moreover, we theoretically investigate ion adsorption mechanisms in the electrodes by comparing experimental data of a CO_2-CDI cell with theoretical results of the classic amphoteric-Donnan model developed for conventional CDI. By comparing the experimental results with the amph-D model, we find that the model overestimates the absorption efficiency in CO_2-CDI experiments. To understand this discrepancy, we investigate the effects of other phenomena, i.e., (i) low ion concentration, (ii) passive CO_2 absorption, and (iii) the effect of acid-base reactions on the chemical surface charge.

Keywords: electrochemical carbon capture; MCDI; carbon electrodes; Donnan model

1. Introduction

Climate change mitigation is one of the major and most urgent challenges that society is facing nowadays. In their 2018 report, the Intergovernmental Panel on Climate Change (IPCC) highlighted the importance of achieving zero CO_2 emissions before 2050 to limit the temperature increase [1]. Among the strategies to reduce CO_2 emissions, CO_2 capture technologies have a major role to play[1,2]. Although a large number of technologies has already been proposed for post-combustion CO_2 capture (e.g., amine sorbents[3–5], calcium looping[6], gas separation membranes[7,8]), there is still an urgent need of novel technologies to capture CO_2 from flue gas and also directly from the atmosphere[9,10]. Recently a new technology has been proposed to capture CO_2 based on membrane capacitive deionization (MCDI)[11]. MCDI is a well-established process based on Capacitive Deionization (CDI), which has been widely used to desalinate water streams [12–20]. A CDI cell is composed of two porous electrodes, which can adsorb ions, either through the formation of an electrical double layer (EDL) in the electrodes[14,15,17] or through ion intercalation[21]. The MCDI cell differs from the CDI cell as the porous electrodes are covered by an ion exchange membrane to improve the salt adsorption performance[20].

MCDI can be used to capture CO_2 in the form of HCO_3^- and CO_3^{2-}. Here, we refer to this technology as CO_2-MCDI. CO_2-MCDI is similar to MCDI, except that the electrolyte solution is a CO_2-sparged water solution instead of a saline solution. When CO_2 gas is sparged in water, CO_2 reacts with water to form carbonic acid ($H_2CO_3^*$), which further dissociates to carbonate ions (HCO_3^- and CO_3^{2-}) until reaching a chemical equilibrium, according to the following reaction [22,23]

$$\mathbf{CO_2(g)} \overset{\mathbf{H^{cc}}}{\leftrightarrow} \mathbf{H_2CO_3^*} \quad (1)$$

$$\mathbf{H_2CO_3^*} \overset{\mathbf{K_1}}{\leftrightarrow} \mathbf{HCO_3^-} + \mathbf{H^+} \quad (2)$$

$$\mathbf{HCO_3^-} \overset{\mathbf{K_2}}{\leftrightarrow} \mathbf{CO_3^{2-}} + \mathbf{H^+} \quad (3)$$

Fig. 1a shows the fraction of each carbon species in solution as function of pH. Fig. 1b illustrates the principles of the CO_2-MCDI cell. By charging the CO_2-MCDI cell, the carbonate ions (CO_3^{2-} and HCO_3^-) are adsorbed in the electrodes EDLs by applying a cell voltage. The resulting concentration decrease of carbonate ions in solution shifts the chemical equilibrium between CO_2 and carbonic acid (Eq.**Error! Reference source not found.**), leading to the absorption of CO_2 gas. At the end of the charging step, CO_2 is adsorbed in the capacitive electrodes ($n_{CO_2(g)}$) in the form of HCO_3^- and CO_3^{2-}, and as a result a CO_2-depleted stream is obtained. The electrode regeneration is achieved by short-circuiting the cell or by discharging

the CO_2-MCDI cell. During this discharge step, the overall process is reversed: the carbonate ions (HCO_3^- and CO_3^{2-}) are desorbed from the electrodes, leading to CO_2 desorption from the solution to the gas phase.

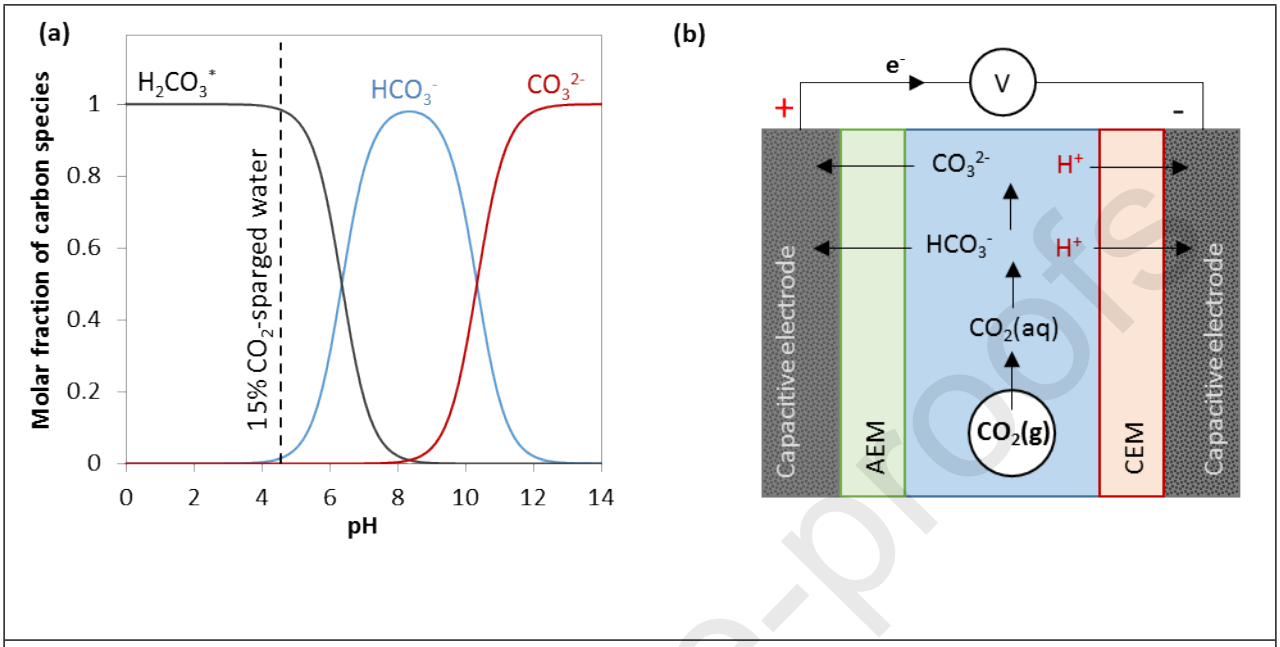

Fig. 1. (a) Fraction of chemical species as function of the solution pH (Bjerrum plot) for the H_2O-CO_2 system at 25°C. The curves are calculated according to Eqs. (1-3) with equilibrium constants H^{cc}=0.83 (ref:[22]), $K_1=10^{-6.35}$ M (ref [23]) and $K_2=10^{-10.33}$ M (ref [23]). (b) Schematic representation of CO_2 capture in a CO_2-MCDI cell. During the charging step, a charging voltage is applied between the electrodes, leading to the adsorption of HCO_3^- and H^+ into the electrodes, and the absorption of gaseous CO_2 in water.

In conventional MCDI for water desalination, the salt absorption performance is reported by the charge efficiency, Λ, which is for a monovalent salt given by $\Lambda=n_{salt}/n_{charge}$[24], where n_{salt} is the amount of salt adsorbed and n_{charge} is the molar charge stored in the electrodes. Ideally, Λ is equal to 1, which indicates that for every electron transferred, one cation and one anion are adsorbed (in case of a monovalent salt). In CO_2-MCDI, we aim to remove CO_2 gas, and likewise conventional MCDI, the performance of a CO_2-MCDI cell can be measured by the absorption efficiency ($\Lambda_a= n_{CO_2(g)})/ n_{charge}$)[11].

In CO_2-MCDI operated at constant current, we found values of Λ_a in the range of 0.6-0.8[11]. Such values of Λ_a are comparable with Λ in conventional MCDI for water desalination[19]. However, we unexpectedly found lower values of Λ_a by charging the CO_2-MCDI cell with lower current densities (from ~0.8 at 0.6 A m^{-2} to ~0.6 at 0.2 A m^{-2}) [11]. A decrease of Λ in conventional MCDI is mainly caused by co-ion expulsion [20,24–26] and by faradaic reactions [27–29]. However, both effects are assumed to be negligible in CO_2-MCDI due to (i) the low

concentration of ions, (ii) the absence of reactive species in solution (e.g., O_2 and Cl^-)[11], and (iii) the presence of ion exchange membranes [20,28,30]. Therefore, the behavior of a CO_2-MCDI cell seems to be different from a conventional MCDI cell operated for water desalination.

Conventional MCDI and CO_2-MCDI only differ by their electrolyte, i.e., CO_2-sparged water solution for CO_2-MCDI and salt solution for MCDI, which mainly differ by their electrolyte strength. On the one hand, an NaCl solution consists of fully dissociated salt, thus being a strong electrolyte. On the other hand, the CO_2-sparged solution contains amphoteric ions (HCO_3^-), thus being a weak electrolyte. To the best of our knowledge, very few studies describe the performance of an MCDI cell with amphoteric ions[11,31–34], i.e., HPO_4^-[35] and HCO_3^- [11,32–34]. Most of these studies describe the performance of an MCDI cell with solutions composed of amphoteric ions in combination with salt ions[32–35], whereas only one study tested the MCDI cell performance with a solution consisting exclusively of amphoteric ions[11]. A CO_2-sparged water solution can have a significant impact on the MCDI performance. For instance, we previously stressed the importance of the pH inside the electrode EDLs for CO_2-sparged solutions[11]. A higher pH inside the anode EDL could lead to the dissociation of HCO_3^- into CO_3^{2-}, which is not desired as the adsorption of CO_3^{2-} requires twice the number of electrons compared to the adsorption of HCO_3^- (Λ_a=0.5 for 1 CO_3^{2-} removed), and therefore Λ_a decreases. Besides, chemisorption of H_2CO_3* could also take places on the electrode surface. CO_2 gas is known to react with porous electrodes, even when the electrodes are not electrically charged[36,37]. Moreover, recent studies showed that $H_2CO_3^*$ could even be adsorbed in porous electrodes by charging a CDI cell with Na^+ and Cl^- ions, a process which has been referred to supercapacitive swing adsorption (SSA)[32–34]. Besides the role of the electrodes, the ion exchange membranes (IEMs) can potentially affect Λ_a. Studies demonstrated the importance of IEMs on the ion selectivity in MCDI cells [38,39], an effect of which was never investigated in CO_2-MCDI with a CO_2-sparged solution.

Compared to a monovalent solution, CO_2-MCDI is a more complex system due to the multitude of physical phenomena (ion adsorption, ion transport in IEMs, gas absorption, and chemical reactions). Therefore, in this work, we separately study the effect of the electrodes and IEMs on the absorption efficiency. In the first part, the role of IEMs on the CO_2-MCDI performance was investigated by performing CO_2 absorption experiments in CO_2-MCDI (i.e., with an AEM and a CEM), in CO_2-AEM-CDI (with only the AEM), in CO_2-CEM-CDI (with only the CEM) and without membranes (CO_2-CDI). In the second part, the HCO_3^-/CO_3^{2-} adsorption mechanisms in the electrodes were theoretically investigated by comparing experimental data with the amphoteric Donnan model (amph-D model). In conventional MCDI using salt solutions, theoretical models have been widely used to predict the salt adsorption in the capacitive electrodes. Finally, in the last part, different possible effects on the HCO_3^-/CO_3^{2-} adsorption in the electrodes were investigated, i.e., (i) the passive CO_2 adsorption in the

electrodes, (ii) the effect of low ion concentrations, and (iii) the chemical dissociation effect of the chemical surface groups in the electrode micropores.

2. Theory

This section describes two theoretical models adopted to predict the performance of a CO_2-CDI cell, operated with a CO_2-sparged solution, and a conventional CDI cell with NaCl solutions. The first model is the so-called amphoteric Donnan (amph-D) model developed by Gao et al.[14] for conventional CDI, while the second model is the multi-equilibria amphoteric Donnan (m-amph-D) model. The m-amph-D model was based on the model proposed by Hemmatifar and Oyarzun et al.[40,41] for conventional CDI. The amph-D model is an extended version of the Donnan model[15], which considers the presence of immobile chemical charge on the carbon surface, the amount of which is assumed to be constant and not dependent on local (electrical) charge and pH. Instead, in the multi-equilibria amph-D model, the amount of chemical surface charge is a function of the local pH at the carbon surface, where the chemical surface charge can vary based on acid-base reactions. Besides the amph-D model, note that other similar models were developed for predicting salt adsorption in conventional CDI, namely, the modified Donnan (mD) model [20] and the improved Donnan (i-mD) model [15]. Among these models, the amph-D model describes the physics and chemistry of ion adsorption in EDLs most realistically. The amph-D model can accurately describe adsorption in a wide range of experimental conditions [42], and can predict phenomena observed under specific conditions including inverted CDI behavior [14,43]. Therefore, we selected the amph-D model in this study.

2.1. Amphoteric Donnan (amph-D) model

The amph-D model considers that the micropores are separated into two different regions, i.e., an acidic region (region A) and a basic region (region B). The acidic region is covered by negatively chemical surface charged groups, i.e. COO^-, and the basic region is covered by positively chemical surface charged groups, i.e. H^+, as shown in Fig. 2. Thus, ion adsorption occurs in 4 different regions (i.e., regions A and B in both cathode and anode). For each region, three different types of charge are considered: the electrical charge (σ_{elec}), the ionic charge (σ_{ionic}) and the chemical surface charge (σ_{chem}).

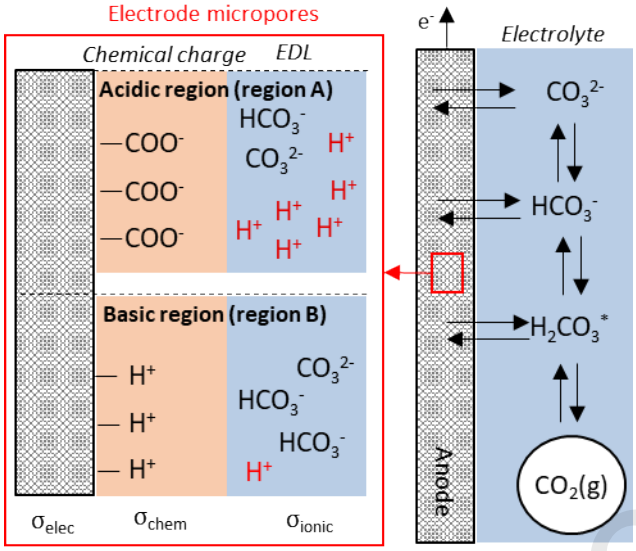

Fig. 2. Schematic illustration of the acidic (region A) and basic regions (region B) in the anode micropores.

In each region, the summation of the three different types of charge is equal to zero, as given by

$$\sigma_{\mathrm{chem,r}} + \sigma_{\mathrm{elec,r}} + \sigma_{\mathrm{ionic,r}} = 0 \tag{4}$$

where subscript r refers to the region (A or B). The ion adsorption in the micropores is related to the Donnan potential[18,44,45], and therefore, the ion concentration in the micropores is given by the Boltzmann equation

$$c_{\mathrm{i,mi,r}} = c_{\mathrm{i}} \cdot e^{-z_{\mathrm{i}} \cdot \Delta\phi_{\mathrm{D}}} \tag{5}$$

where $c_{\mathrm{i,mi,r}}$ refers to the ion concentration in the micropores for each region, c_{i} is the ion concentration in the spacer channel (bulk solution), z_{i} is the ion valence and $\Delta\phi_{\mathrm{D}}$ is the Donnan potential at the interface of the electrode micropore and the solution. In conventional CDI for water desalination, $c_{\mathrm{i,mi,r}}$ usually refers to the concentration of Na^+ or Cl^- [42,46]. Instead, in CO_2-CDI, $c_{\mathrm{i,mi,r}}$ refers to the concentration of HCO_3^-, CO_3^{2-}, H^+, OH^-, $H_2CO_3^*$. The total ionic charge (σ_{ionic}) in each electrode region can be calculated using

$$\sigma_{\mathrm{ionic,r}} = \sum_{\mathrm{i}} z_{\mathrm{i}} \cdot c_{\mathrm{i,mi,r}}. \tag{6}$$

The electrode charge (σ_{elec}) is directly related to the Stern potential ($\Delta\phi_{\mathrm{S}}$) and the Stern capacitance ($C_{\mathrm{s,0}}$), and is given by

$$\sigma_{elec,r} = \frac{\Delta\phi_{S,r} \cdot V_T \cdot C_{s,0}}{F} \quad (7)$$

where V_T is the thermal voltage, and F is the Faraday constant (96485 C mol^{-1}). All potentials are dimensionless, which can be converted to a dimensional voltage by multiplying the dimensional potential with the thermal voltage, $V_T = (R \cdot T)/F$, where R is the ideal gas constant (8.314 J K^{-1} mol^{-1}), and T is the temperature (298 K).

The electrode potential ($\Delta\phi_{elec}$) is defined as the sum of the Stern and Donnan potentials. Furthermore, the potential of each electrode is equal for the regions A and B, and is given by

$$\Delta\phi_{elec} = [\Delta\phi_D + \Delta\phi_S]_A = [\Delta\phi_D + \Delta\phi_S]_B. \quad (8)$$

In equilibrium, there is no potential gradient across the electrodes and the flow channel due to ionic and electronic resistances. Therefore, the (dimensional) cell voltage (V_{cell}) is the difference of the electrode potential between the cathode and anode

$$V_{cell} = (\Delta\phi_{elec,anode} - \Delta\phi_{elec,cathode}) \cdot V_T. \quad (9)$$

We consider that the mass of both electrode regions (A and B) is the same, and therefore we can calculate the average electrode charge ($\sigma_{elec,av}$) using

$$\sigma_{elec,av} = \frac{1}{2} \cdot (\sigma_{elec,A} + \sigma_{elec,B}). \quad (10)$$

For the CO_2-CDI cell, the chemical dissociation constants of the chemical reactions shown in (1(3 must also be included in the amph-D model, as well as chemical dissociation constants (see Table 1).

Table 1: Equilibrium dissociation constants between CO_2(g), H_2CO_3*, HCO_3^-, CO_3^{2-}, OH^-, H^+

Equation	Equilibrium Constant	Reference
$H^{cc} = \frac{C_{H_2CO_3^*}}{C_{CO_2(g)}}$	H^{cc}=0.83	[22]
$K_1 = \frac{C_{HCO_3^-} \cdot C_{H^+}}{C_{H_2CO_3^*}}$	K_1=10$^{-6.35}$	[23]
$K_2 = \frac{C_{CO_3^{2-}} \cdot C_{H^+}}{C_{HCO_3^-}}$	K_2=10$^{-10.33}$	[23]
$K_w = C_{OH^-} \cdot C_{H^+}$	K_w=10^{-14}	

The total carbon (n_T) in the system is distributed through the liquid volume and the gas volume, and is given by

$$n_T = C_T \cdot V_l + m_{elec} \cdot \alpha \cdot V_{mi} \cdot \left(\sum_{r=A,B}^{anode} C_{T,mi,r} + \sum_{r=A,B}^{cathode} C_{T,mi,r} \right) + \frac{P_{CO_2(g)} \cdot V_g}{R \cdot T} \quad (11)$$

where C_T is the concentration of total carbon ($C_T = C_{H_2CO_3^*} + C_{HCO_3^-} + C_{CO_3^{2-}}$), $C_{T,mi}$ is the concentration of total carbon in the micropores, V_{mi} is the micropore volume (mL g_{elec}^{-1}), m_{elec} is the mass per electrode (g $elec^{-1}$), α is the fraction of each micropore region, V_l is the volume of the CO_2-sparged solution, and V_g is the volume of gas. Note that the volume of micropores was measured by a gas adsorption analyzer, which we will discuss in Section 3.2.

For the CO_2-CDI cell with NaCl solutions, the mass balance for the total amount of Na^+ ($n_{total,Na}$) and Cl^- ($n_{total,Cl}$) in the system is

$$n_{total,Na} = c_{Na} \cdot V_l + m_{elec} \cdot \alpha \cdot V_{mi} \cdot \left(\sum_{r=A,B}^{anode} c_{Na,mi,r} + \sum_{r=A,B}^{cathode} c_{Na,mi,r} \right) \quad (12)$$

$$n_{total,Cl} = c_{Cl} \cdot V_l + m_{elec} \cdot \alpha \cdot V_{mi} \cdot \left(\sum_{r=A,B}^{anode} c_{Cl,mi,r} + \sum_{r=A,B}^{cathode} c_{Cl,mi,r} \right). \quad (13)$$

2.2. Multi-equilibria Amphoteric-Donnan (m-amph-D) model

In contrast to the amph-D model, the m-amph-D model considers that the chemical surface charge is dependent on the local pH at the carbon surface. Studies showed that the chemical surface charge can change over time, due to the local pH at the carbon surface [41], or due to electrode oxidation reactions [47]. Since the pH is expected to change drastically in both electrodes, as H^+ is the only cation present in solution, we implement a similar approach as developed in ref[41] to describe the chemical surface charge as function of pH. We consider the acid-base groups A^-/AH, for the acidic region, and BH^+/B, for the basic region, and their dissociation constants K_A and K_B, respectively. K_A and K_B, which are given by

$$K_A = \frac{C_{A^-} \cdot C_{H,mi,A}}{C_{AH}} \quad (14)$$

$$K_B = \frac{C_B \cdot C_{H,mi,B}}{C_{BH^+}}. \quad (15)$$

Then, we can substitute $c_{A^-} = -\sigma_{chem,A}$ and $c_{BH^+} = \sigma_{chem,B}$. The total concentration of surface groups is then given by $\sigma_{chem,A,tot} = -(c_{A^-} + c_{AH})$ and $\sigma_{chem,B,tot} = c_{BH^+} + c_B$. Consequently, we can express $\sigma_{chem,A}$ and $\sigma_{chem,B}$ in the m-amph-D model as

$$\sigma_{\mathrm{chem,A}} = \frac{K_A}{K_A + C_{H,mi,A}} \cdot \sigma_{\mathrm{chem,A,tot}} \quad (16)$$

$$\sigma_{\mathrm{chem,B}} = \frac{C_{H,mi,B}}{K_5 + C_{H,mi,B}} \cdot \sigma_{\mathrm{chem,B,tot}} \ . \quad (17)$$

3. Material and methods

3.1. Electrode and cell preparation

In this work, we selected two types of carbon electrodes, i.e., carbon cloth (CC) and activated carbon (AC) electrodes. The CC electrodes are commercially available (ACC-5092-15, Kynol, Germany), and the AC electrodes were home-made according to a previously reported method[48,49]. In this method, a slurry was prepared from two components: I) activated carbon (DLC, super 30, Norit, the Netherlands, BET=1600 m^2 g^{-1}), II) a solution of N-Methyl-2-pyrrolidone (NMP) and polyvinylidene fluoride (PVDF) (KYNAR HSV 900, Arkema Inc., USA) in a ratio of 30:1 (w/w). The slurry was then casted on a graphite sheet with a 500 µm-thickness casting knife, and dried for 24 h. After evaporation, the fabricated electrodes were then composed of 10 wt% PVDF and 90 wt% AC with a thickness of 200 µm. Then, the electrodes were soaked in deionized water for at least 24 hours to remove all traces of ions initially present in the electrodes. The MCDI cell was composed of several layers, i.e., (i) titanium coated with platinum current collector, (ii) the AC electrode, (iii) a CEM (CMX, Astom (Neosepta), Japan), (iv) a polymeric spacer (PA 6.6 fabric, Nitex 03-300/51, Sefar, Switzerland, 200 µm), (v) an AEM (AMX, Astom (Neosepta), Japan) and (vi) another AC electrode and a current collector. The CDI cell has the cell structure than the MCDI cell except than the AEM and CEM layers. Moreover, the CDI cell was also tested with the CC electrodes.

3.2. Electrode characterization

Porosity analysis, SEM images, and titration were performed on each type of electrode (CC and AC electrodes). Porosity analyses were performed using an automated gas adsorption analyzer (Tristar 3000, micromeritics Instrument Corp., USA). Prior to the analysis, a sample of 0.2 g of electrodes material was dried at 598 K under N_2 atmosphere. Then, an N_2 isotherm was obtained at 77 K using 0.1 g of dry sample of AC electrodes and 0.2 g of dry sample of CC electrodes. The pore-size distribution was then calculated from the N_2 isotherm data using the non-localized density functional theory (NLDFT) model, provided by the built-in software of the instrument (Fig. 3c). The volume of micropores was then found by integrating the pore volume with a diameter smaller than 2 nm.

Titration was performed with an automated titration station (888 Titrando, Methrom). Before titration, 50 mL of 0.05 M NaOH solution was constantly sparged with N_2 to remove all traces of dissolved CO_2. Then, an electrode sample (0.5 g for the AC electrode and 1 g for the CC electrode) was soaked in the NaOH solution, and then titrated by dosing 0.5 mL of acid solution (0.1 M HCl) every 3-5 min. The time for each dosing step was adjusted to reach a stable pH value, which indicates that the electrode reached a chemical equilibrium with the solution. During the titration period, the NaOH solution was constantly sparged with N_2 to avoid the presence of CO_2 and the effect thereof on the titration results. A blank titration was performed following the same procedure, without the electrode sample. The results of the blank and sample titrations are shown in the supporting information (Fig. S2). For each pH value measured, the concentration of chemical charge on the carbon surface is calculated using

$$\sigma_{\mathrm{chem,pH}} = \frac{(\mathrm{V_{sample}} - \mathrm{V_{blank}}) \cdot \mathrm{C_{titrant}}}{\mathrm{V_{mi}} \cdot \mathrm{m_{electrode}}} \tag{18}$$

where $\mathrm{C_{titrant}}$ represents the concentration of the titrant (HCl), $\mathrm{V_{mi}}$ the micropore volume per electrode mass, $\mathrm{m_{electrode}}$ the mass of the electrodes used during titration, $\mathrm{V_{sample}}$ the titrant volume obtained from the sample titration at a given pH value, and $\mathrm{V_{blank}}$ the titrant volume obtained from the blank titration at a given pH value.

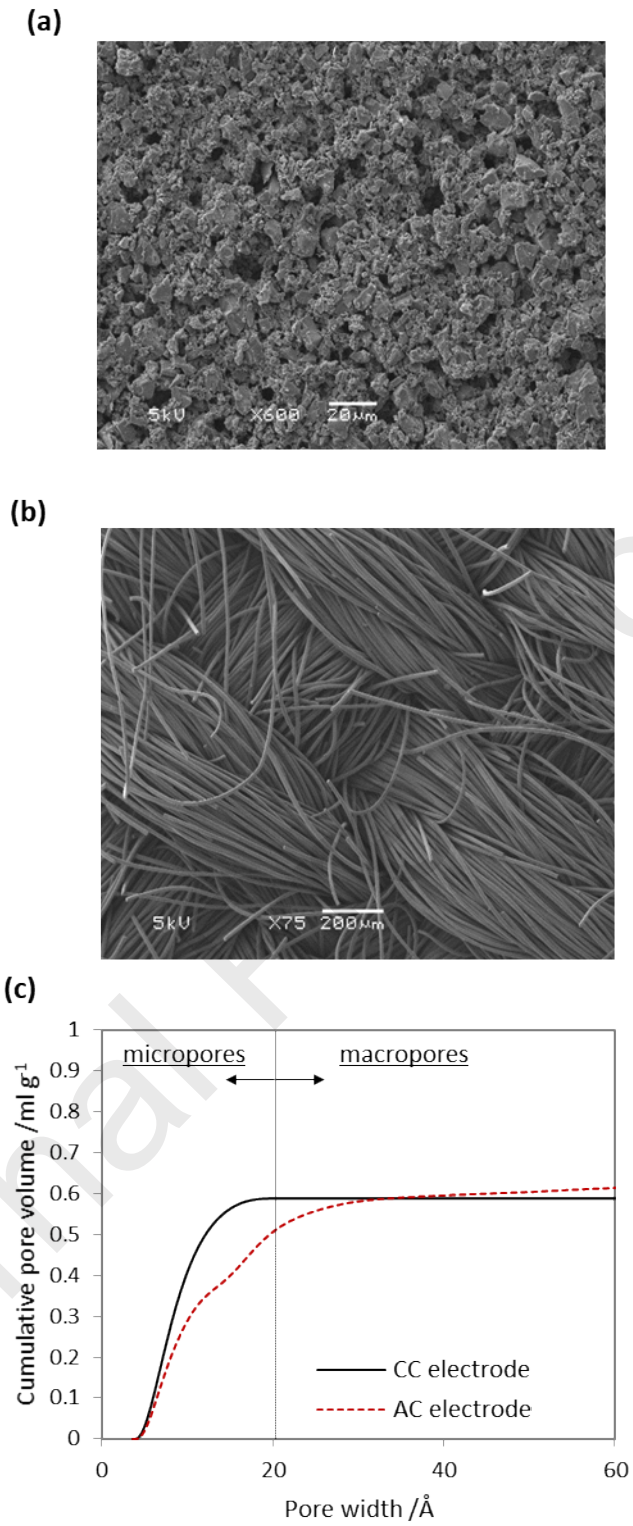

Fig. 3. Electrode characterization of the AC and CC electrode materials: SEM image of the (a) AC and (b) CC electrode, and (c) porosity analysis for the AC and CC electrodes. The pores with a diameter smaller than 20 Å (2 nm) are considered as micropores, while the pores with a diameter larger than 20 Å are considered as macropores.

Fig. 3a-b show the microscopic structure of the electrode materials. The AC electrode (Fig. 3a) shows a homogeneous porous structure, whereas the CC electrode consists of carbon fibers.

3.3. Experimental procedure for passive CO_2 absorption in uncharged electrodes

The CO_2 absorption in the electrodes was characterized in the absence of an electrical field in absorption batch experiments. We refer to this type of experiment as "passive CO_2 absorption". A similar experiment has been previously done with NaCl[15] or with mixtures of salts[50,51].The passive CO_2 absorption experiments were performed in batch mode using a home-made reactor. The home-made reactor consisted of a glass flask, which contained a CO_2:N_2 gas mixture (V_g=55 mL) and a CO_2-sparged deionized water solution (V_l=90 mL). Prior to each experiment, the deionized water was equilibrated with a defined CO_2 partial pressure (the same as in the gas phase) by flushing a CO_2:N_2 gas mixture into the reactor. At the same time, the electrode material was pre-treated in two steps. In the first step, the electrode material was soaked into deionized water, and sparged with N_2 for 20 hours. In the second step, the electrode material was dried at room temperature for 4 hours. During the experiment, the pre-treated electrode material was submerged in the reactor (solution phase), while all the gas valves were closed. The amount of carbon species adsorbed in the electrode material was monitored by measuring the gas pressure with a manometer (Cerabar T PMP131, Endress+Hauser). The change of gas pressure is directly related to a change of CO_2 partial pressure, since N_2 is inert in the system, and is not expected to be adsorbed in the electrode. From the change of gas pressure, the total amount of carbon species adsorbed in the electrodes ($C_{total}=CO_2(g)_+H_2CO_3^*+HCO_3^-+H^+$) is calculated based on a carbon mass balance and the chemical equilibrium reactions as given by Eqs. 1-3.

3.4. (M)CDI experiment procedure

Charging/discharge cycles were performed with (M)CDI cells using both CO_2-sparged (CO_2 absorption tests) and NaCl solutions (salt adsorption tests). During the charging step, a current (or voltage) was applied between the electrodes to adsorb ions from the solution. During the discharge step, a reversed current or a discharge voltage of 0 V was applied between the electrodes to desorb ions into the solution. The two following sections describe the procedures for the salt adsorption and the CO_2 absorption experiments.

3.4.1. Salt adsorption with NaCl solutions (conventional CDI)

Salt adsorption tests were performed in CDI cells using different NaCl concentrations (0.1, 0.5, 1, 5, and 20 mM) in batch experiments until reaching equilibrium. The research set-up consisted of a CDI cell and a glass bottle stirred with a magnetic stirrer. A peristaltic pump (Masterflex L/S, Cole-Parmer, USA) was used to recirculate an NaCl solution between the CDI cell and the glass bottle at a flow rate of 40 mL min^{-1}. The water volume was different in each experiment to ensure that the ion adsorption in the CDI cell did not lead to a complete depletion

of NaCl in solution. Charging/discharge cycles were applied to the CDI cell. During the charging step, a constant voltage of 0.3, 0.5, 0.7 or 1V was applied to the CDI cell, while during the discharge step, a constant voltage of 0V was applied. The charging time, which was equal to the discharge time, was long enough to ensure that the CDI cell reached an equilibrium. Since only NaCl was present in solution, the amount of salt removed from the solution was monitored by measuring the conductivity of the solution. The charge efficiency was calculated as

$$\Lambda = \frac{n_{Na^+(ad)} + n_{Cl^-(ad)}}{n_{charge}} = \frac{(C_{NaCl,initial} - C_{NaCl,final}) \cdot F}{Q} \quad (19)$$

where Q is the electrical charge stored in the electrode, $c_{NaCl,initial}$ is the NaCl concentration at the beginning of a charging step, and $c_{NaCl,final}$ is the NaCl concentration at the end of a charging step.

3.4.2. CO_2 absorption tests (CO_2-(M)CDI)

Several CO_2-(M)CDI experiments were performed in batch mode using the same procedure as previously reported in ref [11]. Before the experiment, a CO_2-sparged water solution was prepared by flushing a gas mixture of N_2:CO_2 (85%:15% vol/vol) using two mass flow controllers (MASS-STREAM D-6300, Bronkhorst, the Netherlands) in deionized water. A volume of the CO_2-sparged solution (33 mL) was circulated at 30 mL min^{-1} between the (M)CDI cell and a gas-liquid contactor (GLC). Both the (M)CDI cell and the GLC were contained in a controlled-temperature chamber at 298K. The GLC is a cylinder-shaped glass container, which contains both a gas and a liquid phase, and ensures the exchange of CO_2 between both phases. Note that the recirculated solution and the gas phase in the GLC were sparged with the same gas mixture (15% CO_2) until both phases reach chemical equilibrium. At the same time, the MCDI cell was short-circuited (cell voltage of 0 V) to reach a chemical equilibrium between the ion concentrations in the micropores and in the CO_2-sparged solution. After the entire system reached an equilibrium, gas valves were closed to enclose a defined volume of gas in the GLC. The experiment started by charging the CO_2-(M)CDI cell either in constant current or constant voltage mode. In constant current mode, a current density (0.2, 0.4, or 0.6 A m^{-2}) was applied between the electrodes, both during galvanostatic charging (positive current) and discharge (negative current). Under constant voltage mode, a cell voltage of 0.3, 0.5, 0.7 or 1 V was applied during charging, and a cell voltage of 0 V was applied during discharge. Different times for charging and discharge were tested (1.1 h, 2h, and 5h). A potentiostat (Ivium, the Netherlands) was used to control the current or the voltage. During the experiment, the relative pressure of the gas in the GLC was monitored with a manometer (Cerabar T PMP131, Endress+Hauser). Based on the change of the partial CO_2 pressure during the experiment (ΔP_{CO_2}), the amount of CO_2 absorbed or desorbed during one cycle was estimated with the ideal gas law as

$$\Lambda_a = \frac{n_{CO_2(g)}}{n_{charge}} = \frac{\Delta P_{CO_2} \cdot F}{Q \cdot R \cdot T}. \quad (20)$$

The energy consumption (W^*_{net}) was calculated based on the energy consumption of the (M)CDI cell (W_{net}) and the amount of CO_2 gas absorbed

$$W^*_{net} = \frac{W_{net}}{n_{CO_2}} = \frac{\int_0^{\infty} V^c_{cell} dQ - \int_0^{\infty} V^D_{cell} dQ}{n_{CO_2}} \quad (21)$$

where V^c_{cell} is the cell voltage during charging, V^D_{cell} the voltage during discharge, and Q is the electrical charge stored.

4. Results and discussion

4.1. Absorption efficiency in CO_2-MCDI

Firstly, we characterized the absorption efficiency in a CO_2-MCDI cell at constant current under various conditions (different current densities, amount of charge stored, and cycle times). Fig. 4a shows the electrical charge and the pressure measured during typical adsorption/desorption cycles in CO_2-MCDI operated in constant current mode. As can be seen from Fig. 4a, the gas pressure in the gas-liquid contactor decreases, when the electrical charge stored in the electrodes increases, and vice-versa. This charge-pressure relationship illustrates the principle of the CO_2-MCDI cell: by increasing the amount of charge stored in the electrode, carbonate ions (HCO_3^- and CO_3^{2-}) are electro-adsorbed in the anode and removed from the electrolyte solution. Consequently, the carbonate ion concentration decreases in the electrolyte solution, and more CO_2 gas is spontaneously absorbed in the electrolyte solution (according to equilibrium reactions given by Eqs. 1-3).

Fig. 4b-d show the absorption efficiency (Λ_a) as function of the charge stored in the electrodes (Fig. 4b), the current density (Fig. 4c), and the charging time (Fig. 4d). In our previous study[11], Λ_a was already characterized as function of current density. However, the effect of current density could not be differentiated from other effects (the charge stored in the electrodes and the charging time). Fig. 4b-d show that Λ_a tends to decrease with longer charging times (e.g., from Λ_a=0.55 after 1 hour to Λ_a=0.35 after 4.5 hours), while no specific relation is found with the electrode charge and the current density. This observation is in good agreement with our previous study (Λ_a=0.7 for 0.7 hours and Λ_a=0.5 for 3.3 hours) [11]. In ref[11], we hypothesized that a decrease of Λ_a with longer cycle time could be related to the selective adsorption of CO_3^{2-} in the electrodes at longer charging times. Time-dependent selective adsorption of divalent ions in capacitive electrodes has been shown in conventional CDI[25]. However, besides the electrode behavior, the IEMs could also influence Λ_a. For instance, the IEMs show a selectivity towards specific ions based on their valence[39,52] or

size[52]. The individual effect of the electrodes and the IEMs is challenging to distinguish in CO_2-MCDI experiments. Therefore, we investigated the individual effect of the IEMs and the capacitive electrodes by characterizing Λ_a with (CO_2-MCDI) and without IEMs (CO_2-CDI).

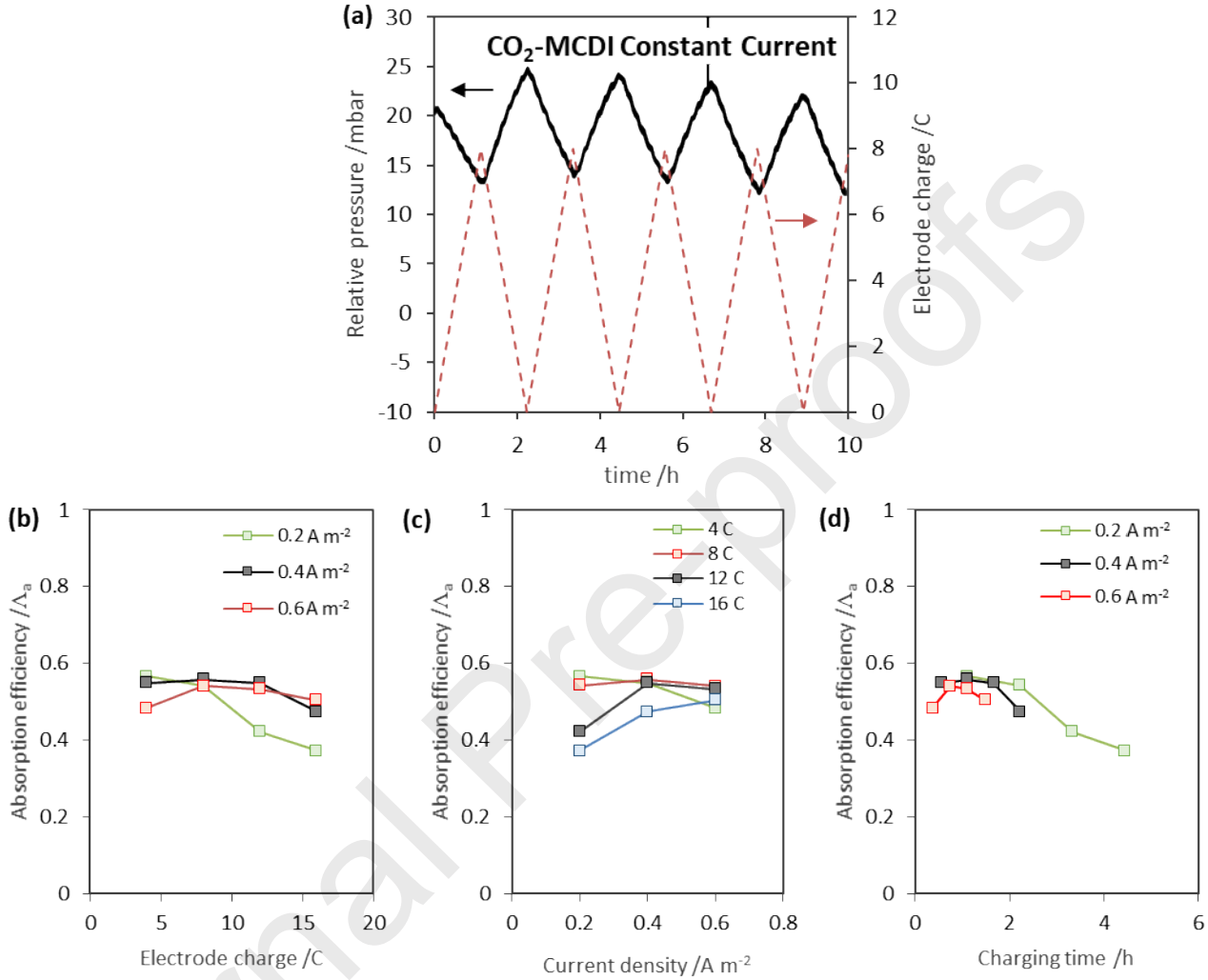

Fig. 4. (a) Gas pressure in the gas-liquid contactor (GLC) and the charge stored in the electrode of the CO_2-MCDI cell operated in constant current mode (0.4 A m^{-2} until 8 C). Absorption efficiency ($\boldsymbol{\Lambda_a}$) as function of the (b) charge, (c) current density, and (d) charging time. Lines are added to guide the eye.

4.2. Effect of membranes on CO_2 absorption in CO_2-MCDI

Fig. 5 shows the values of Λ_a for CO_2-MCDI and for CO_2-CDI as function of the current density (Fig. 5a), cell voltage (Fig. 5b), and charging time (charging voltage of 0.5 V) (Fig. 5c). Fig. 5a shows that values of Λ_a are clearly higher in CO_2-MCDI compared to CO_2-CDI in constant current mode (Λ_a≈0.55 for CO_2-MCDI compared to Λ_a≈0 for CO_2-CDI). These findings are in line with results expected from conventional MCDI for water desalination. In conventional MCDI for water desalination, the IEMs greatly improve the charge efficiency (Λ) by blocking

the desorption of co-ions from the electrode macropores[19,20]. Unexpectedly, CO_2-CDI experiments show no significant CO_2 absorption at 0.2 and 0.4 A m^{-2}. While the charge efficiency (Λ) in conventional CDI suffers from co-ion expulsion [20,24–26] and faradaic reactions [27,29,47], we assume that both of these effects are negligible in CO_2-CDI. On the one hand, the effect of co-ion expulsion decreases at lower ion concentrations[19,24]. The concentration of ions in the feed water in CO_2-CDI is very low (≈0.05 mM), more than 400 times lower than ion concentrations usually tested in CDI (i.e., typically 20 mM NaCl). On the other hand, faradaic reactions in conventional CDI are mostly related to the presence of dissolved O_2 gas and of Cl^-, both of which are absent in a CO_2-sparged solution.

To study ion adsorption mechanisms in the electrodes, we performed experiments in constant voltage mode (Fig. 5b). In constant voltage mode, a chemical equilibrium in the electrode EDLs is reached when all time-dependent phenomena vanish. In contrast, the current mode controls the flux of ions, which continually drives several time-dependent processes (ionic flux, chemical reaction, ion adsorption, etc.). Like the constant current mode, Fig. 5b shows that values of Λ_a are higher in CO_2-MCDI than CO_2-CDI, independent of the charging voltage. Nevertheless, Fig. 5c shows that the values of Λ_a in CO_2-MCDI decrease with charging time (Λ_a≈0.51 at 1 h against Λ_a≈0.35 at 5.5 h), which was not the case for CO_2-CDI. These results demonstrate that the CO_2-MCDI cell did not reach equilibrium even after 5 hours. Fig. 5d shows that the CO_2 concentration in CO_2-MCDI experiments never reached a stable value during charging and discharge, which demonstrates that a net CO_2 flux still occurs in the system. Unlike the CO_2-MCDI cell, the CO_2-CDI cell reached equilibrium after 1 hour, as values of Λ_a in CO_2-CDI are stable with time from 1 hour (Fig. 5c), and Fig. 5d shows that a constant CO_2 concentration is reached in both the charging and discharge steps. Therefore, the decrease in Λ_a observed at a longer time in CO_2-MCDI (described in section 4.1) is mostly caused by the presence of IEMs, and not directly from the electrode adsorption behavior. This finding disproves the hypothesis we made in ref[11], where we presumed that the loss of Λ_a in CO_2-MCDI with time was related to the electrode behavior.

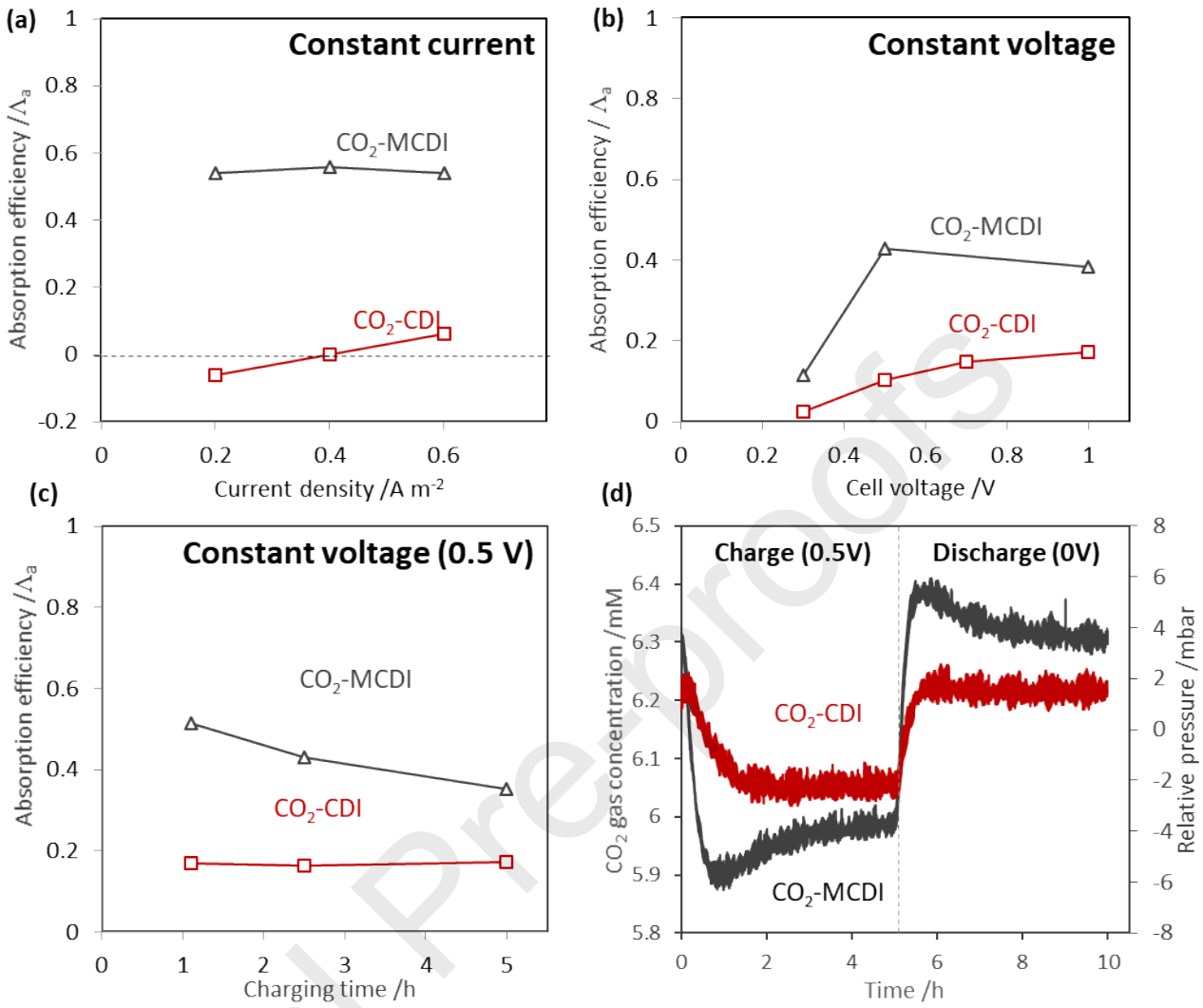

Fig. 5. Absorption efficiency of CO_2 in CO_2-MCDI (grey line) and CO_2-CDI configurations (red line) at (a) constant current (0.2-0.6 A m^{-2} by applying 8 C), (b) at constant voltage (0.3-1 V during 2.2 hours) and (c) at constant voltage with different charging times (0.5 V between 1.1 hours and 5 hours). (d) Gas pressure in CO_2-MCDI (grey line) and CO_2-CDI configurations (red line) at 0.5 V for 5 hours charging.

Since the membrane pair influences the CO_2-MCDI performance, it is not possible to differentiate the individual effect of either the AEM or CEM from the CO_2-CDI and CO_2-MCDI alone. To that end, we performed experiments with a cell by including only an AEM or a CEM, both in constant current and constant voltage mode (Fig. 6). Fig. 6a shows that higher values of Λ_a were obtained by using only an AEM compared to using only a CEM in both modes (Λ_a ≈0.49 with CO_2-AEM-CDI and Λ_a≈0.24 with CO_2-CEM-CDI in constant current operation, see Fig. 6). Moreover, using only one AEM gives similar values of Λ_a as in CO_2-MCDI, where both IEMs are used (Λ_a=0.54 with CO_2-MCDI and Λ_a=0.49 with CO_2-AEM-CDI in constant current operation, see Fig. 6). Fig. 6b also shows similarities between the CO_2-AEM-CDI and CO_2-MCDI cells in terms of CO_2 concentration profile with time (at 0.5V), which suggests that the

CO_2-AEM-CDI did not reach equilibrium either. Instead, the CO_2-CEM-CDI cell shows a similar behavior than CO_2-CDI at constant voltage (Fig. 6a-b). Therefore, the higher values of Λ_a from the CO_2-MCDI cell are mainly due to the presence of the AEM. The CO_2 concentration as function of time for the CO_2-AEM-CDI suggests that a concentration gradient builds up across the AEM during charging (and discharge) with time (Fig. 6b). For instance, Fig. 6b shows that the CO_2 concentration first decreases during the charging step, but then starts to increase after one hour. We believe that, upon charging the cell, more carbonate ions (HCO_3^-/CO_3^{2-}) migrate through the AEM to the macropores of the anode than the amount that is adsorbed in the micropores of the anode. As a result, HCO_3^- and CO_3^{2-} ions accumulate in the anode macropores, increasing the total carbon concentration (C_T=HCO_3^-+CO_3^{2-}+$H_2CO_3^*$) in the macropores of the anode. Driven by the total carbon concentration difference between the anode macropores and the spacer solution, the total carbon diffuses from the macropores to the spacer solution. This total carbon flux can occur through the (i) diffusion of $H_2CO_3^*$ or (ii) the combined transport of HCO_3^- and H^+ due to the co-ion leakage of H^+.

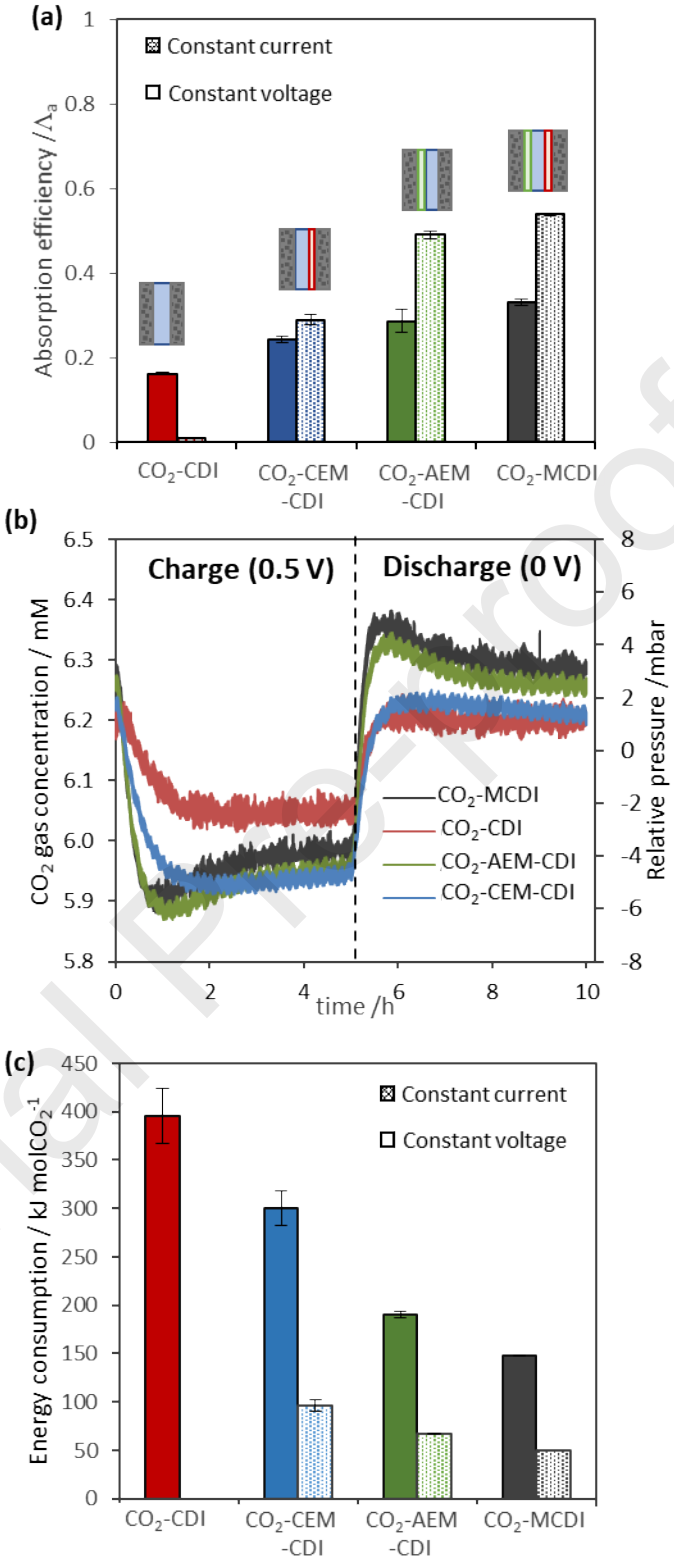

Fig. 6. Absorption efficiency of CO_2 in different CDI configurations: CO_2-MCDI, CO_2-AEM-CDI, CO_2-CEM-CDI, and CO_2-CDI (a) at constant voltage (0.5 V at 5 hours charging) and constant current (0.4 A m^{-2}, maximum charge 8 C). (b) Pressure and CO_2 gas concentration at 0.5 V. (c) Energy consumption at 0.5 V and 0.4 A m^{-2}.

As clearly shown in Fig. 6a, ion exchange membranes (in particular the AEM) are essential to keep a high absorption efficiency (Λ_a) in CO_2-MCDI. Achieving a high Λ_a is mostly essential to minimize the energy consumption[11]. Fig. 6c shows that the lowest energy consumption was achieved with the CO_2-MCDI cell at constant current (W^*_{net}=49 kJ molCO_2^{-1} for CO_2-MCDI), the configuration in which the highest Λ_a was obtained. In contrast, the highest energy consumption was obtained with the CDI cell at constant voltage (W^*_{net}=390 kJ molCO_2^{-1} for CO_2-CDI), the configuration in which the lowest Λ_a was obtained. Covering the electrode with an ion exchange membrane (MCDI) is a suitable strategy to increase Λ_a, and also to decrease the energy consumption. The CDI performance was much lower than expected (compared to conventional CDI), with a maximum absorption efficiency of only 0.18 in constant voltage mode (Fig. 6b). As a first step toward developing a theoretical model for CO_2-MCDI, we will theoretically investigate the ion adsorption mechanism in CO_2-CDI at equilibrium condition (time independent) in the next section. A full MCDI model is more complex than a CO_2-CDI equilibrium model as a MCDI model not only includes time-independent phenomena (ion adsorption in electrode micropores) but also time-dependent phenomena (ions transport in electrode macropores, membranes and spacer). Thus, developing a reliable model for CO_2-CDI is essential before developing a more complex CO_2-MCDI model.

Studying the system under equilibrium conditions (i.e., constant voltage at long charging time) is essential to understand the system behavior before modelling CO_2-MCDI cells. Besides equilibrium condition in the micropores, MCDI model also include time-dependent phenomena.

4.3. CO_2-CDI results compared with theoretical models

4.3.1. Conventional amphoteric-Donnan model

Understanding ion adsorption mechanisms in CO_2-CDI cell is of primary importance in order to optimize the process performance. In this section, we theoretically investigate the adsorption mechanisms by comparing the amphoteric Donnan (amph-D) model[14,42] with experimental data. To the best of our knowledge, the amph-D model has been extensively used for NaCl solutions[26,40,53,54], but never for CO_2-sparged solutions. We performed CO_2-CDI experiments with two different carbon materials, i.e., activated carbon (AC) and carbon cloth (CC) electrodes. Prior to our modeling work, we performed a CDI experiment with a NaCl solution (see Fig. S3 in supporting information) to determine three model parameters, namely, the Stern capacitance in the zero-charge limit (Cs_0), and the chemical surface charge in the acidic and basic regions ($\sigma_{chem,A}$, $\sigma_{chem,B}$). Finally, the electrode micropore volume was determined by porosity analysis, as shown in Fig. 3c. The parameter values for both electrode materials are shown in Table 2.

Table 2: Parameters used in the amph-D model for both electrode materials

	AC electrode	CC electrode
$\mathbf{V_{mi}}$ (mL/g_{elec})	0.5	0.6
$\mathbf{m_{elec}}$ (g_{elec}/electrode)	0.5	0.9
$\boldsymbol{\alpha}$	0.5	0.5
$\mathbf{Cs_0}$ (F/mL)	170	170
$\boldsymbol{\sigma_{chem,A}}$ (mM)	-620	-710
$\boldsymbol{\sigma_{chem,B}}$ (mM)	400	350

Fig. 7 shows a comparison between the experimental data and the theory of the absorption efficiency as function of cell voltage. The model correctly predicts the increase of the adsorption efficiency with increasing voltage, but overestimates the value of Λ_a. Fig. 8a shows the relative effect of the adsorption of HCO_3^-, the expulsion of H^+ and the adsorption of CO_3^{2-} in/from the micropores of the anode on Λ_a. A non-ideal absorption efficiency (Λ_a<1) can be caused by both (i) the adsorption of CO_3^{2-} and (ii) the expulsion of H^+, which are, in this particular case, underestimated by the amph-D model. Adsorption of CO_3^{2-} is hardly predicted by the amph-D model as the predicted pH in the micropores by the model (maximum of pH≈8) is lower than the pH value where HCO_3^- dissociate into CO_3^{2-} (pH>9 see Fig. 1a). The amph-D model does not describe the CO_2 adsorption accurately with the parameter values reported in Table 2, which were found by fitting the theory to experimental data of salt adsorption in desalination experiments.

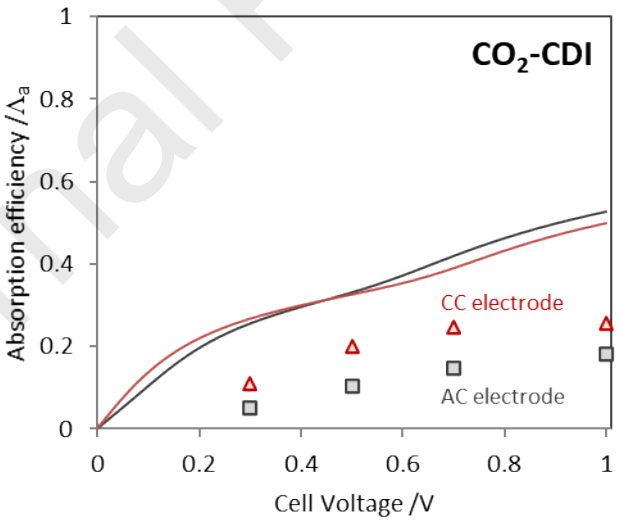

Fig. 7. CO_2 absorption efficiency calculated by the amph-D model (line) compared with experimental data (symbols) obtained in CO_2-CDI experiments as function of cell voltage for (a) activated carbon (AC) and (b) carbon-cloth (CC) electrodes.

This discrepancy between data and theory can be the result of several factors. Firstly, the ionic strength of CO_2-sparged solutions is lower than of the NaCl solutions used in the CDI experiments. (< 1 mM NaCl). However, the amph-D model describes the data fairly well at low ions concentration, also shown in SI. Secondly, the concentration of the neutral molecule

$H_2CO_3^*$ in is the highest in the electrolyte. As $H_2CO_3^*$ is a weak acid, and only the dissociated species HCO_3^- and CO_3^{2-} can be electrosorbed, chemical equilibria (Eq. 1-3) can have a strong effect on the absorption performance, and these equilibria are dependent on the local pH in the micropores. Thirdly, chemisorption of $H_2CO_3^*$ at the carbon surface can affect the absorption performance.

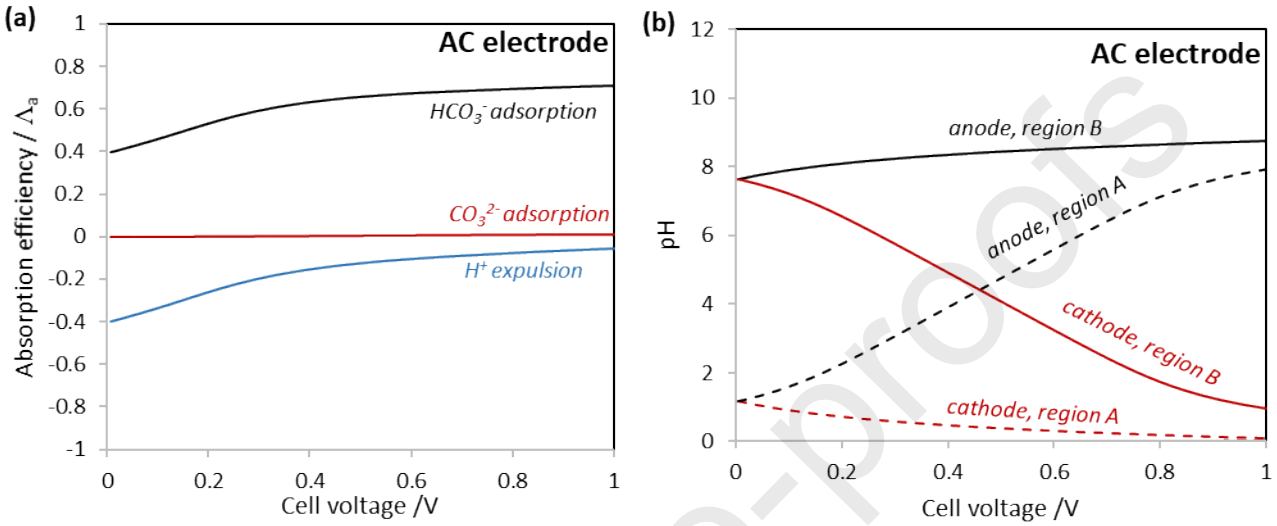

Fig. 8. (a) Effect of H^+ expulsion, and of HCO_3^- and CO_3^{2-} adsorption in the anode calculated by the amph-D model for the AC electrode. (b) pH calculated in the micropores of the anode and cathode for the acidic (region A) and basic region (region B) for the AC electrode.

We investigate the chemisorption of CO_2 at the electrode material by CO_2 absorption experiments with uncharged electrodes in the absence of an electric field. Ref. [40] and [51] study the effect of chemisorption of specific chemical species (mostly NO_3^-) on ion adsorption and include a new parameter in the amph-D model to describe this effect (intrinsic selectivity coefficient[40] or affinity term[51]). Fig. 9 shows the experimental and calculated amount of total carbon (C_{total}=CO_2(g)+$H_2CO_3^*$+HCO_3^-+CO_3^{2-}) adsorbed by uncharged electrodes as function of the CO_2 partial gas pressure. The amph-D model predicts the CO_2 adsorption in uncharged AC carbon material well, which suggests that no significant CO_2 chemisorption takes place in the AC electrodes. On the other hand, the amph-D model underestimates the amount of CO_2 adsorbed by the CC electrode material. This finding suggests that CO_2 chemisorption seems to occur in the CC electrode material. CO_2 chemisorption can occur through the chemical affinity between specific chemical surface groups and CO_2, such as amine groups[5].

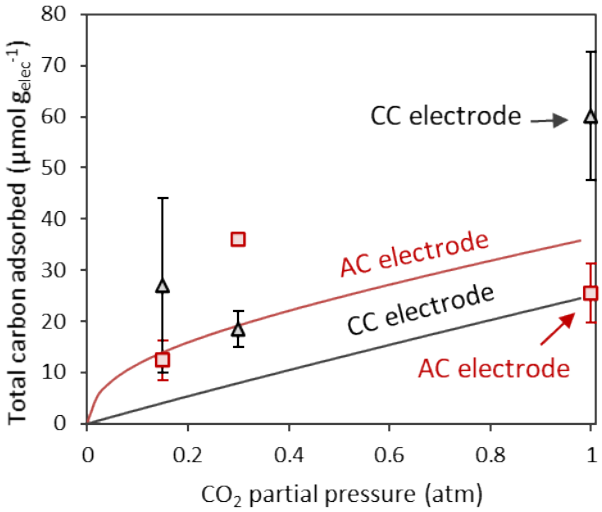

Fig. 9. Comparison between model predictions (lines) and experimental data (symbols) for passive adsorption with CC and AC electrodes material at different CO_2 partial pressures. Error bars show standard deviation.

4.3.2. Multi-equilibria amphoteric-Donnan model

In the previous sections we discussed that the amph-D model does not perfectly describe the CO_2 absorption performance of the CDI cell. We will now consider the chemical surface charge at the carbon electrodes as weak acid-base groups, which dissociate according to a dissociation equilibrium constant, especially when strong pH changes occur during charging and discharge. Furthermore, we will run, on both electrode materials, titration experiments in order to determine the amount of chemical surface charge. ~~T~~To include the effect of pH changes in the conventional amph-D model, we adopted the modeling approach from Hemmatifar et al., and we use a "multi-equilibria amphoteric Donnan" (m-amph-D) model[41]. The m-amph-D model requires at least two additional fitting parameters, i.e., a minimum of one dissociation constant for the acidic group (K_A) and one dissociation constant for the basic group (K_B). Moreover, the m-amph-D requires the total amount of surface groups ($\sigma_{chemA,tot}$ and $\sigma_{chemB,tot}$), instead of only the chemical surface charge of the amph-D model (σ_{chemA} and σ_{chemB}). To find parameter values for m-amph-D model, including the dissociation constants and chemical surface charge parameters, titration experiments were performed (see Supporting information for more details on the fitting procedure) [41]. Fig. 10a-b show the m-amph-D fit with the fitting parameters shown in Table 3 to the chemical surface charge obtained from experimental electrode titrations. Fig. 10c-d show the chemical surface charge as function of pH in the regions A and B of the electrodes. Values of the chemical surface charge used for the amph-D (Table 2) and m-amph-D models (Table 3) are different, but are hardly comparable due to the different theoretical models. A similar difference between values of σ_{chem} obtained from electrode titration and the amph-D model was reported by Gao et al.[14].

Table 3: parameters used in the titration model

	AC electrode	CC electrode
$\sigma_{chemA,tot,1}$ (mM)	-1300	-800
$\sigma_{chemA,tot,2}$ (mM)		-500
$\sigma_{chemB,tot}$ (mM)	400	1300
$pk_{a,1}$ (mM)	2	2
$pk_{a,2}$ (mM)	N/A	9
pk_b (mM)	>12	8

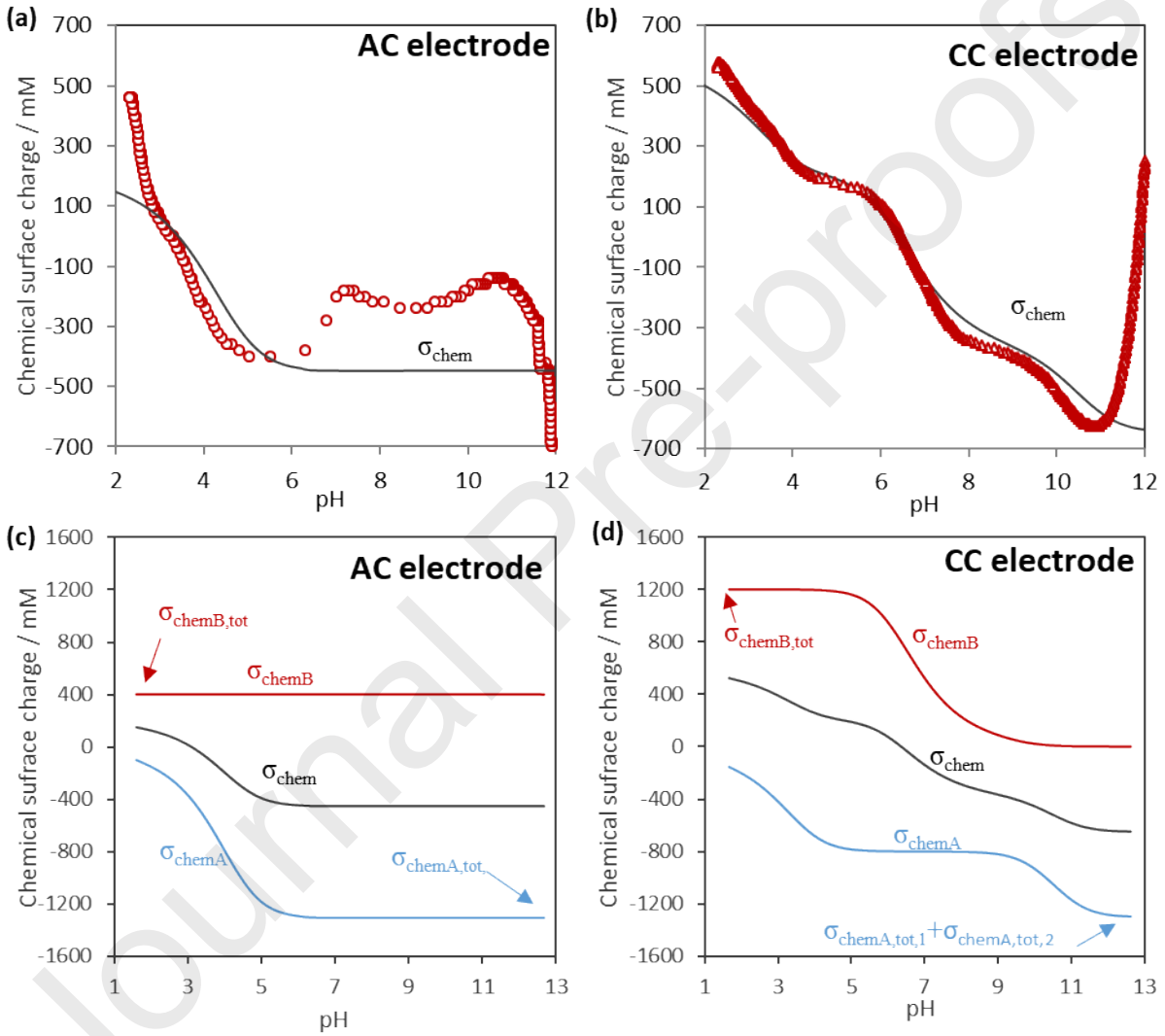

Fig. 10: Experimental data fitted with a titration model describing the total chemical surface charge as a function of pH for the (a) AC electrodes and (b) the CC electrodes. The data points are based on electrode titration experiments. Chemical surface charge in region A (σ_{chemA}) and region B (σ_{chemB}) for the (c) AC electrodes and (d) the CC electrodes.

Fig. 11a-b show a comparison between the absorption efficiency as function of the cell voltage obtained from both models (amph-D model and the m-amph-D model) and the experimental data. In comparison with the amph-D model, the m-amph-D model shows a better fit with the experimental data obtained from the AC electrode. Regarding the CC electrode, the m-amph-D model improves overall the fit with the experimental data but underestimates the absorption efficiency at cell voltages below 1 V.

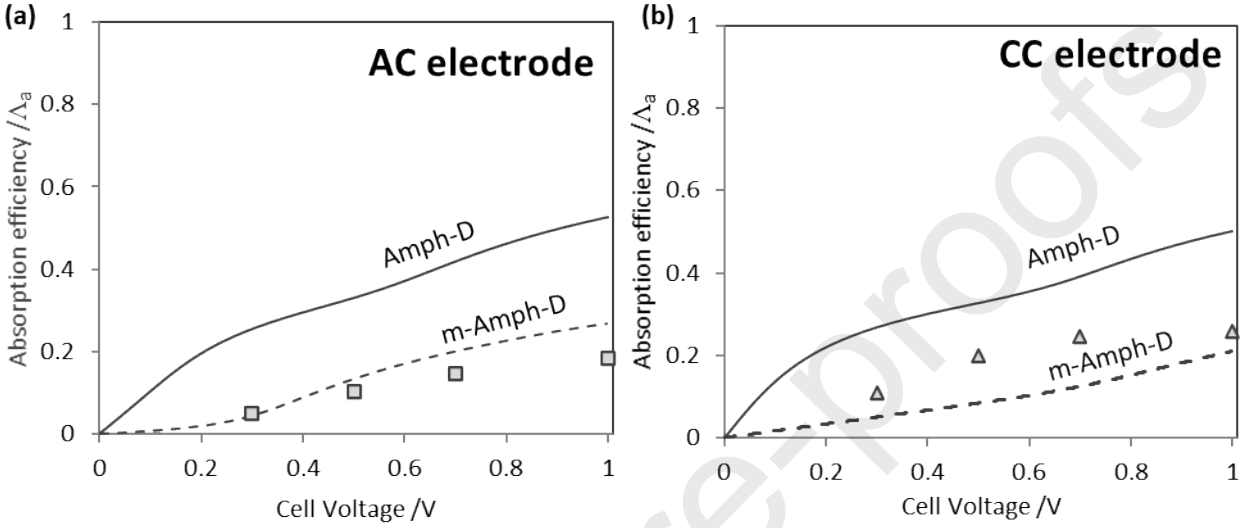

Fig. 11. Comparison between the amph-D and m-amph-D models and the experimental data obtained with (a) AC electrodes and (b) CC electrodes.

While the AC and CC electrode materials show similar material properties in terms of pore-size distribution and Stern capacitance in the zero-charge limit (see Table 1), the CC electrode differs from the AC electrode in terms of surface chemistry. The AC and CC electrodes also differ in terms of morphology (Fig. 3a-b). However, we believe that the electrode morphology has no significant effect on the adsorption performance in equilibrium conditions: the electrode morphology would mainly influence the dynamics of ion transport from the macropores to the micropores of the electrode. Titration results suggest that, on the surface of the CC electrode material, more types of chemical surface groups are present than on the AC electrode material (3 pKvalues for the CC electrode against 1 pK value for the AC electrode, see Table 3 and Fig. 10). Moreover, the results of passive CO_2 absorption experiments suggest that CO_2 chemisorption takes place in the CC electrode micropores (Fig. 9), which indicates the presence of specific chemical surface groups with an affinity for the carbon species. For instance, a chemical affinity of CO_2 with amine groups is reported in Ref. [3,55]. We believe that the presence of both types of chemical surface groups can lead to more complex interactions with adsorbed carbonate ions, which are not predicted by the m-amph-D model yet.

Other effects not considered in this study could also influence the absorption efficiency, e.g., (i) the ion size-based selectivity[40] and (ii) the non-ideal dissociation degree in the micropores of the EDL. Regarding size-based selectivity, monovalent ions with lower hydrated radius (i.e., K^+ and Na^+[58]) and/or a lower ion hydration ratio[59] have been shown to be selectively adsorbed in the electrode EDLs from monovalent salt mixtures (e.g. with K^+ and Na^+). However, to the best of our knowledge, no study clearly defines the hydrated radius of HCO_3^-, and therefore, we cannot estimate the effect of size-based selectivity between HCO_3^- and CO_3^{2-}. Besides the ion-size based selectivity effects, the dissociation constant of carbonate species (H_2CO_3* and HCO_3^-) in the micropores of the electrode and of chemical surface charge could be dependent on the electrical field. According to the dissociation field-effect theory[56,57], the dissociation of an acid increases under the presence of an electric field in EDLs, mainly due to a change of permittivity conditions. Thus, we can hypothesize that the dissociation constants of bicarbonate ions (HCO_3^-/CO_3^2) can increase with cell voltage, resulting in a higher amount of CO_3^{2-} adsorbed in the electrode EDLs at a given pH, leading to lower absorption efficiencies. Moreover, the chemical surface charge in the acidic region (region A) can vary in a similar way according to the same dissociation field effect theory. In a broader context, a better understanding of chemical interactions in electrode micropores in the presence of an electrical field is of great interest to tune the selectivity of carbon materials towards certain ions in CDI.

5. Conclusions

In this work, we investigated the role of the membranes and electrodes on the CO_2-MCDI performance by testing different CDI configurations, i.e., with and without membranes. Moreover, we theoretically investigated ion adsorption in electrodes (CO_2-CDI) by comparing the amph-D model with experimental data. CO_2-MCDI cells show the highest absorption efficiencies and the lowest energy consumption among the investigated CDI configurations. We demonstrated that the improved performance of CO_2-MCDI compared to CO_2-CDI can be mostly attributed to the presence of the AEM in the cell, whereas the CEM contributes less. The AEM improves the absorption efficiency by ensuring that only bicarbonate and carbonate ions are transported to the anode during charging, and by hindering the transport of expulsed co-ions (H^+) from the anode to the spacer solution. Although the presence of the AEMs in the CO_2-MCDI cell improves the performance, the absorption efficiency decreases with increasing charging time. At longer charging time, we observe that carbon is transported from the anode back to the spacer channel, which can be explained by (i) co-ion leakage (H^+ and HCO_3^-) due to the high mobility of H^+ and by (ii) the diffusion of neutral molecules ($H_2CO_3^*$). Therefore, to optimize the performance, shorter cycles are preferred in a CO_2-MCDI configuration. Beyond the role of the membranes, we show that the absorption efficiency in CO_2-CDI is lower than prediction by the amph-D model. To explain the discrepancy between theory and data, three

different effects were investigated, i.e., (i) chemisorption of CO_2, (ii) the low ion concentrations, and (iii) the acid-base dissociation of the chemical surface groups. A better fit was obtained between the experimental data and a new version of the amph-D model, the so-called multi-equilibria Amphoteric Donnan model, which includes a description of acid-base dissociation reactions of the chemical surface groups was incorporated. We demonstrated that these processes affect the performance of the CO_2-CDI system. Future work should focus on investigating and differentiating physical (by employing porous electrodes with no chemical surface charge) and chemical effects (by employing porous electrodes with chemical surface charge) of weak electrolyte solutions in CDI, especially by investigating the effect of the electrical field on the chemical dissociation constant of weak acids, and on the chemical surface charge in the EDLs.

Author contributions

The manuscript was written through the contributions of all authors. In particular, L. Legrand et Q. Shu performed the experimental work, and L. Legrand et J.E. Dykstra performed the modeling work.

Acknowledgments

This work was performed in the cooperation framework of Wetsus, European Centre of Excellence for Sustainable Water Technology (www.wetsus.eu). Wetsus is co-funded by the Dutch Ministry of Economic Affairs and Ministry of Infrastructure and Environment, the Province of Fryslân, and the Northern Netherlands Provinces. Moreover, the authors are grateful to the participants of the research theme “Sustainable Carbon Cycle” for fruitful discussions and financial support.

Appendix A. Supplementary material

Supplementary data to this article can be found online at:

References

[1] P.R.S. Masson-Delmotte, V., P. Zhai, H.-O. Pörtner, D. Roberts, J. Skea, M.I.G. A. Pirani, W. Moufouma-Okia, C. Péan, R. Pidcock, S. Connors, J.B.R. Matthews, Y. Chen, X. Zhou, and T.W. E. Lonnoy, T. Maycock, M. Tignor, ICCP report (summary for policymarkers), 2018.

[2] I.E.A. International, E. Agency, Energy Technology Perspectives 2017, (2017). doi:10.1787/energy_tech-2017-en.

[3] R. Dugas, G. Rochelle, Absorption and desorption rates of carbon dioxide with monoethanolamine and piperazine, Energy Procedia. 1 (2009) 1163–1169. doi:10.1016/j.egypro.2009.01.153.

[4] B. Dutcher, M. Fan, A.G. Russell, Amine-Based CO 2 Capture Technology Development from the Beginning of 2013 □ A Review, (2015). doi:10.1021/am507465f.

[5] M. Parvazinia, S. Garcia, M. Maroto-valer, CO2 capture by ion exchange resins as amine functionalised adsorbents, Chem. Eng. J. 331 (2018) 335–342. doi:10.1016/j.cej.2017.08.087.
[6] C.C. Dean, J. Blamey, N.H. Florin, M.J. Al-Jeboori, P.S. Fennell, The calcium looping cycle for CO2 capture from power generation, cement manufacture and hydrogen production, Chem. Eng. Res. Des. 89 (2011) 836–855. doi:10.1016/j.cherd.2010.10.013.
[7] R. Khalilpour, K. Mumford, H. Zhai, A. Abbas, G. Stevens, E.S. Rubin, Membrane-based carbon capture from fl ue gas : a review, J. Clean. Prod. 103 (2015) 286–300. doi:10.1016/j.jclepro.2014.10.050.
[8] S. Rafiq, L. Deng, M. Ha, Role of Facilitated Transport Membranes and Composite Membranes for Efficient CO 2 Capture – A Review, (2016) 68–85. doi:10.1002/cben.201500013.
[9] D.W. Keith, G. Holmes, D.S. Angelo, K. Heidel, A Process for Capturing CO2 from the Atmosphere, Joule. 54 (2017) 32–37. doi:10.1016/j.joule.2018.05.006.
[10] E.S. Sanz-Pérez, C.R. Murdock, S.A. Didas, C.W. Jones, Direct Capture of CO2from Ambient Air, Chem. Rev. 116 (2016) 11840–11876. doi:10.1021/acs.chemrev.6b00173.
[11] L. Legrand, O. Schaetzle, R.C.F. De Kler, H.V.M. Hamelers, Solvent-Free CO2Capture Using Membrane Capacitive Deionization, Environ. Sci. Technol. 52 (2018) 9478–9485. doi:10.1021/acs.est.8b00980.
[12] J.E. Dykstra, P.M. Biesheuvel, H. Bruning, A. Ter Heijne, Theory of ion transport with fast acid-base equilibrations in bioelectrochemical systems, Phys. Rev. E - Stat. Nonlinear, Soft Matter Phys. 90 (2014) 1–10. doi:10.1103/PhysRevE.90.013302.
[13] X. Gao, A. Omosebi, N. Holubowitch, J. Landon, K. Liu, Capacitive Deionization Using Alternating Polarization: Effect of Surface Charge on Salt Removal, Electrochim. Acta. 233 (2017) 249–255. doi:10.1016/j.electacta.2017.03.021.
[14] X. Gao, S. Porada, A. Omosebi, K.L. Liu, P.M. Biesheuvel, J. Landon, Complementary surface charge for enhanced capacitive deionization, Water Res. 92 (2016) 275–282. doi:10.1016/j.watres.2016.01.048.
[15] P.M. Biesheuvel, S. Porada, M. Levi, M.Z. Bazant, Attractive forces in microporous carbon electrodes for capacitive deionization, J. Solid State Electrochem. 18 (2014) 1365–1376. doi:10.1007/s10008-014-2383-5.
[16] S. Porada, R. Zhao, A. Van Der Wal, V. Presser, P.M. Biesheuvel, Review on the science and technology of water desalination by capacitive deionization, Prog. Mater. Sci. 58 (2013) 1388–1442. doi:10.1016/j.pmatsci.2013.03.005.
[17] J.E. Dykstra, S. Porada, A. Van Der Wal, P.M. Biesheuvel, Energy consumption in Capacitive Deionization – constant current versus constant voltage operation, Water Res. (2018) 1–12. doi:10.1016/j.watres.2018.06.034.
[18] V. Der Wal, 2011_J.Colloid.Int.Sci._Theory of Membrane capacitive deionization including the effect of the electrode pore space.pdf, 360 (2011).
[19] R. Zhao, P.M. Biesheuvel, A. Van Der Wal, Energy consumption and constant current operation in membrane capacitive deionization, Energy Environ. Sci. 5 (2012) 9520–9527. doi:10.1039/c2ee21737f.
[20] P.M. Biesheuvel, R. Zhao, S. Porada, A. van der Wal, Theory of membrane capacitive deionization including the effect of the electrode pore space, J. Colloid Interface Sci. 360 (2011) 239–248. doi:10.1016/j.jcis.2011.04.049.
[21] S. Porada, P. Bukowska, A. Shrivastava, P.M. Biesheuvel, K.C. Smith, Nickel Hexacyanoferrate Electrodes for Cation Intercalation Desalination, Arxiv: 1612.08293. (2017) 1–16. doi:10.1016/j.electacta.2017.09.137.
[22] R. Sander, Compilation of Henry's law constants (version 4.0) for water as solvent, Atmos. Chem. Phys. 15 (2015) 4399–4981. doi:10.5194/acp-15-4399-2015.
[23] X. Wang, W. Conway, R. Burns, N. McCann, M. Maeder, Comprehensive study of the hydration and dehydration reactions of carbon dioxide in aqueous solution, J. Phys. Chem. A. 114 (2010) 1734–1740. doi:10.1021/jp909019u.
[24] R. Zhao, P.M. Biesheuvel, H. Miedema, H. Bruning, A. van der Wal, Charge efficiency:

A functional tool to probe the double-layer structure inside of porous electrodes and application in the modeling of capacitive deionization, J. Phys. Chem. Lett. 1 (2010) 205–210. doi:10.1021/jz900154h.

[25] R. Zhao, M. Van Soestbergen, H.H.M. Rijnaarts, A. Van Der Wal, M.Z. Bazant, P.M. Biesheuvel, Journal of Colloid and Interface Science Time-dependent ion selectivity in capacitive charging of porous electrodes, J. Colloid Interface Sci. 384 (2012) 38–44. doi:10.1016/j.jcis.2012.06.022.

[26] P.M. Biesheuvel, H.V.M. Hamelers, M.E. Suss, Theory of Water Desalination by Porous Electrodes with Immobile Chemical Charge, Colloids Interface Sci. Commun. 9 (2015) 1–5. doi:10.1016/j.colcom.2015.12.001.

[27] W. Tang, D. He, C. Zhang, P. Kovalsky, T.D. Waite, Comparison of Faradaic reactions in capacitive deionization (CDI) and membrane capacitive deionization (MCDI) water treatment processes, Water Res. 120 (2017) 229–237. doi:10.1016/j.watres.2017.05.009.

[28] J. Yu, K. Jo, T. Kim, J. Lee, J. Yoon, Temporal and spatial distribution of pH in fl ow-mode capacitive deionization and membrane capacitive deionization, Desalination. 439 (2018) 188–195. doi:10.1016/j.desal.2018.04.011.

[29] P. Nativ, Y. Badash, Y. Gendel, New insights into the mechanism of flow-electrode capacitive deionization, Electrochem. Commun. 76 (2017) 24–28. doi:10.1016/j.elecom.2017.01.008.

[30] D. He, C.E. Wong, W. Tang, P. Kovalsky, T. David Waite, Faradaic Reactions in Water Desalination by Batch-Mode Capacitive Deionization, Environ. Sci. Technol. Lett. 3 (2016) 222–226. doi:10.1021/acs.estlett.6b00124.

[31] X. Huang, D. He, W. Tang, P. Kovalsky, T.D. Waite, Environmental Science Investigation of pH-dependent phosphate removal from wastewaters by membrane capacitive, (2017) 875–882. doi:10.1039/c7ew00138j.

[32] B. Kokoszka, N.K. Jarrah, C. Liu, D.T. Moore, K. Landskron, Supercapacitive swing adsorption of carbon dioxide, Angew. Chemie - Int. Ed. 53 (2014) 3698–3701. doi:10.1002/anie.201310308.

[33] C. Liu, K. Landskron, Design, construction, and testing of a supercapacitive swing adsorption module for CO_2 separation, Chem. Commun. 53 (2017) 3661–3664. doi:10.1039/C7CC01055A.

[34] S. Zhu, K. Ma, K.M. Landskron, Relationships between the Charge-Discharge Methods and the Performance of a Supercapacitive Swing Adsorption Module for CO2Separation, J. Phys. Chem. C. (2018). doi:10.1021/acs.jpcc.8b03968.

[35] X. Huang, D. He, W. Tang, P. Kovalsky, T.D. Waite, Environmental Science Investigation of pH-dependent phosphate removal from wastewaters by membrane capacitive, Environ. Sci. Water Res. Technol. 3 (2017) 875–882. doi:10.1039/c7ew00138j.

[36] M. Younas, M. Sohail, L.K. Leong, M.J. Bashir, S. Sumathi, Feasibility of CO2 adsorption by solid adsorbents: a review on low-temperature systems, Int. J. Environ. Sci. Technol. 13 (2016) 1839–1860. doi:10.1007/s13762-016-1008-1.

[37] M.G. Plaza, S. García, F. Rubiera, J.J. Pis, C. Pevida, Post-combustion CO2capture with a commercial activated carbon: Comparison of different regeneration strategies, Chem. Eng. J. 163 (2010) 41–47. doi:10.1016/j.cej.2010.07.030.

[38] A. Hassanvand, G.Q. Chen, P.A. Webley, S.E. Kentish, A comparison of multicomponent electrosorption in capacitive deionization and membrane capacitive deionization, Water Res. 131 (2018) 100–109. doi:10.1016/j.watres.2017.12.015.

[39] L. Wang, S. Lin, Mechanism of Selective Ion Removal in Membrane Capacitive Deionization for Water Softening, Environ. Sci. Technol. (2019). doi:10.1021/acs.est.9b00655.

[40] D.I. Oyarzun, A. Hemmatifar, J.W. Palko, M. Stadermann, J.G. Santiago, Ion selectivity in capacitive deionization with functionalized electrode : Theory and experimental validation, Water Res. X. 1 (2018) 100008. doi:10.1016/j.wroa.2018.100008.

[41] A. Hemmatifar, D.I. Oyarzun, J.W. Palko, S.A. Hawks, M. Stadermann, J.G. Santiago,

Equilibria model for pH variations and ion adsorption in capacitive deionization electrodes, Water Res. 122 (2017) 387–397. doi:10.1016/j.watres.2017.05.036.

[42] P.M. Biesheuvel, Activated carbon is an electron-conducting amphoteric ion adsorbent, ArXiv. (2015) 1–9. http://arxiv.org/abs/1509.06354.

[43] P.M. Biesheuvel, H.V.M. Hamelers, M.E. Suss, Theory of Water Desalination by Porous Electrodes with Immobile Chemical Charge, Colloids Interface Sci. Commun. 9 (2015) 1–5. doi:10.1016/j.colcom.2015.12.001.

[44] H. Ohshima, S. Ohki, Donnan potential and surface potential of a charged membrane, Biophys. J. 47 (1985) 673–678. doi:10.1016/S0006-3495(85)83963-1.

[45] A.H. Galama, J.W. Post, M.A. Cohen Stuart, P.M. Biesheuvel, Validity of the Boltzmann equation to describe Donnan equilibrium at the membrane-solution interface, J. Memb. Sci. 442 (2013) 131–139. doi:10.1016/j.memsci.2013.04.022.

[46] J.E. Dykstra, K.J. Keesman, P.M. Biesheuvel, A. van der Wal, Theory of pH changes in water desalination by capacitive deionization, Water Res. 119 (2017) 178–186. doi:10.1016/j.watres.2017.04.039.

[47] J. Yu, K. Jo, T. Kim, J. Lee, J. Yoon, Temporal and spatial distribution of pH in fl ow-mode capacitive deionization and membrane capacitive deionization, Desalination. 439 (2018) 188–195. doi:10.1016/j.desal.2018.04.011.

[48] F. Liu, O. Schaetzle, B.B. Sales, M. Saakes, C.J.N. Buisman, H.V.M. Hamelers, Effect of additional charging and current density on the performance of Capacitive energy extraction based on Donnan Potential, Energy Environ. Sci. 5 (2012) 8642–8650. doi:10.1039/c2ee21548a.

[49] H.V.M. Hamelers, O. Schaetzle, J.M. Paz-García, P.M. Biesheuvel, C.J.N. Buisman, Harvesting Energy from CO_2 Emissions, Environ. Sci. Technol. Lett. 1 (2014) 31–35. doi:10.1021/ez4000059.

[50] A. Hemmatifar, D.I. Oyarzun, J.W. Palko, S.A. Hawks, M. Stadermann, J.G. Santiago, Equilibria model for pH variations and ion adsorption in capacitive deionization electrodes, Water Res. 122 (2017) 387–397. doi:10.1016/j.watres.2017.05.036.

[51] T.M. Mubita, J.E. Dykstra, P.M. Biesheuvel, A. Van Der Wal, S. Porada, Selective adsorption of nitrate over chloride in microporous carbons, Water Res. 164 (2019) 114885. doi:10.1016/j.watres.2019.114885.

[52] A. Hassanvand, G.Q. Chen, P.A. Webley, S.E. Kentish, A comparison of multicomponent electrosorption in capacitive deionization and membrane capacitive deionization, Water Res. 131 (2018) 100–109. doi:10.1016/j.watres.2017.12.015.

[53] X. Gao, A. Omosebi, J. Landon, K. Liu, Enhanced Salt Removal in an Inverted Capacitive Deionization Cell Using Amine Modified Microporous Carbon Cathodes, Environ. Sci. Technol. 49 (2015) 10920–10926. doi:10.1021/acs.est.5b02320.

[54] T.M. Mubita, S. Porada, P.M. Biesheuvel, A. van der Wal, J.E. Dykstra, Capacitive deionization with wire-shaped electrodes, Electrochim. Acta. 270 (2018) 165–173. doi:10.1016/j.electacta.2018.03.082.

[55] M. Parvazinia, S. Garcia, M. Maroto-valer, CO2 capture by ion exchange resins as amine functionalised adsorbents, Chem. Eng. J. 331 (2018) 335–342. doi:10.1016/j.cej.2017.08.087.

[56] L. Onsager, Deviations from Ohm's law in weak electrolytes, J. Chem. Phys. 2 (1934) 599–615. doi:10.1063/1.1749541.

[57] G.W. H.W. Nurnberg, Influences on homogeneous chemical reactions in the diffuse double layer, J. Electroanal.Chem. 21 (1969) 99–122.

[58] M.E. Suss, Size-Based Ion Selectivity of Micropore Electric Double Layers in Capacitive Deionization Electrodes, 164 (2017) 270–275. doi:10.1149/2.1201709jes.

[59] Y. Li, C. Zhang, Y. Jiang, T. Wang, H. Wang, Effects of the hydration ratio on the electrosorption selectivity of ions during capacitive deionization, DES. 399 (2016) 171–177. doi:10.1016/j.desal.2016.09.011.

Graphical abstract

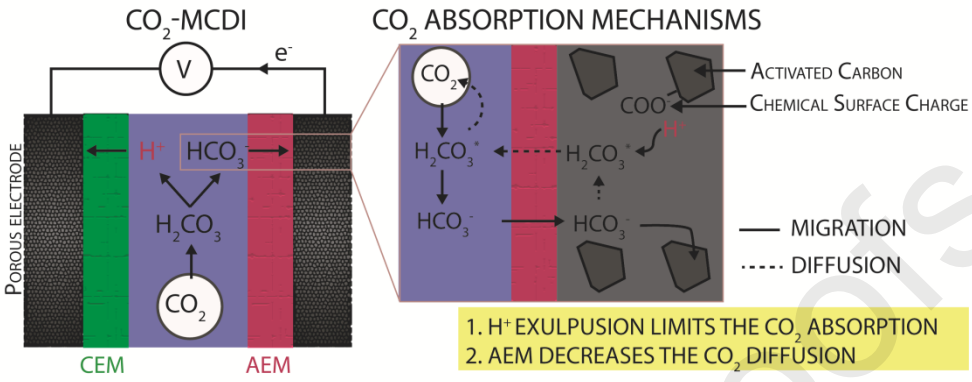

Author contributions

The manuscript was written through the contributions of all authors. In particular, L. Legrand et Q. Shu performed the experimental work, and L. Legrand et J.E. Dykstra performed the modeling work.